AAS 22-111

A MODERN LOAD RELIEF GUIDANCE SCHEME FOR SPACE LAUNCH VEHICLES

Jeb S. Orr* **and Colter W. Russell†**

Launch vehicle load relief algorithms are concerned with realizing a reduction of transient bending moments near maximum dynamic pressure. Traditional approaches to load relief typically use inner-loop acceleration feedback to reduce the wind-induced angle of attack. When implemented in the inner loop, load relief bandwidth is necessarily limited by the achievable stability margins, and when acceleration feedback is employed, by the uncertainty associated with structural modes that couple with the body-mounted accelerometer. The structure of inner-loop load relief increases the dimensionality of the flight control gain and filter optimization problem. Most importantly, classical load relief laws do not take advantage of high-rate and high-accuracy GPS-aided inertial velocity data that is readily available from modern strapdown IMUs.

In this paper, a novel load relief guidance scheme is described that uses direct angle-of-attack feedback in a clever mechanization. The steering commands are determined by examining the wind-perturbed dynamics of a launch vehicle with respect to a gravity turn ascent trajectory. An angle of attack estimate is derived from GPS-aided inertial data and pre-launch range wind measurements, and it is shown that a reduction worst-case rigid-body loads can be realized without requiring air data. The algorithm also includes a high-rate navigation data preprocessing scheme that operates directly on the IMU delta-theta and delta-velocity measurements in order to produce a filtered acceleration estimate at the vehicle center of mass. The outer-loop guidance scheme simplifies the design process for the classical inner-loop autopilot. Algorithm performance is demonstrated using Monte Carlo analysis of a representative liquid booster in a production high-fidelity launch vehicle simulation.

1 INTRODUCTION

Load relief is a control technique designed to reduce transient bending loads in large launch vehicle structures. As structural mass tends toward an optimized minimum to meet structural requirements while maximizing propellant mass fraction, the fundamental longitudinal bending frequencies decrease, challenging the flight control design. Often, the limiting load case for the primary structure of a large launch vehicle is the transient bending due to wind-induced angle of attack, and ascent trajectories and control algorithms are necessarily designed to minimize these effects.

A typical launch vehicle ascent is flown using a *gravity turn*, or a trajectory whose launch-site relative tilt angle χ approximately satisfies the equation

$$\dot{\chi} = \frac{g}{V} \sin \chi \tag{1}$$

*Flight Systems Principal Staff, Mclaurin Aerospace, Knoxville, TN
†Flight Systems Technical Staff, Mclaurin Aerospace, Knoxville, TN

where g is the gravity acceleration and V is the velocity magnitude. This profile, designed offline and determined from a lookup table or polynomial approximation, is shaped such that the turning rate of the vehicle balances the vertical component of gravity and results in no net lateral accelerations. For most launch vehicles, the turning rate $\dot{\chi}$ is on the order of one to two degrees per second. In the absence of wind, it can be shown that attitude profiles that obey Equation 1 result in a nearly zero angle of attack throughout the boost trajectory.

In the presence of wind, the vehicle will experience an angle of attack or sideslip that is approximately proportional to the ratio of the lateral wind velocity and the forward vehicle velocity. If the winds are known *a priori*, for example, via seasonal meteorological models or balloon measurements, the trajectory shape itself can be modified prior to flight using a technique called wind biasing. This approach, even using seasonal winds data from large-scale atmosphere models, can significantly improve launch availability by reducing the predicted distribution of the induced transient loads.

However, such approaches do not account for uncertainty in the actual wind field versus that predicted or measured prior to flight. In order to further reduce in-flight bending loads, it is necessary to estimate the vehicle angle of attack based on its measurable dynamic states, and drive the angle of attack toward zero. For launch vehicles, the primary control objective is reduction of the product of dynamic pressure and total angle of attack, or $\bar{q}\alpha_T$. While this is a rigid-body load metric, it is commonly used as a surrogate for the actual bending moments on the vehicle structure. Since launch vehicles approaching atmospheric regions of maximum gust activity are typically at transonic or supersonic velocities, the ability of a control scheme to respond to short-period gusts (e.g., gust penetration) is limited when typical large rocket flight control system bandwidths have time constants on the order of 5 seconds and the lowest vehicle bending modes are near 1 Hz. As such, designers tend to focus on mitigating quasi-steady winds.

It is noted that reducing $q\alpha_T$ does not always imply reduced bending moments when the fully coupled aeroelastic vehicle system is considered. In fact, for some long and slender launch vehicles, moments due to gimbaling can dominate over aeroelastic loads. In this paper, only rigid-body load relief approaches are considered.

2 HISTORICAL METHODS

Most load relief algorithms use some form of angle of attack feedback or surrogate normal acceleration (N_z) feedback. Since direct measurement of angle of attack is difficult to implement in practice, a knowledge of the vehicle aerodynamic characteristics, particularly the normal force partial $C_{N\alpha}$, can be used to deduce a control signal that is related to angle of attack based on inputs from a body-mounted accelerometer. This approach, or some variant of it, has been used on nearly all load relief schemes for large orbital boost systems, including NASA's Saturn I/IB, Space Shuttle, Space Launch System, and so on. However, this approach is limited in bandwidth due structural bending and the fact that in launch vehicles, accelerometers must often be located far forward or aft of the center of mass.

Using classical notation for the pitch plane control law of a simplified, rigid-body rocket, the simplest N_z feedback algorithm has the form

$$\beta_c = -k_p\phi_y - k_d\omega_y - k_z\ddot{z}_B \tag{2}$$

where ϕ_y is the pitch perturbation from the reference trajectory, ω_y is the body angular rate about the pitch axis, and $\ddot{z}_B$ is the normal acceleration expressed in body coordinates. The commanded

gimbal angle β_c is determined from proportional-derivative (PD) feedback using the gains k_p and k_d for the proportional and derivative gains, respectively, and the accelerometer feedback k_z is used to augment the feedback control.

Assuming a rigid, symmetric vehicle, no sloshing propellant, a perfect actuator, and no servoelastic coupling, the linearized vehicle dynamics in the pitch plane are given by the coupled system of differential equations

$$I_{yy}\dot{\omega}_y = N_\alpha X_{cp}\alpha + X_G F_R \beta_c \tag{3}$$

$$m_T \ddot{z}_I = -m_T \bar{g}\phi_y - N_\alpha \alpha - F_R \beta_{Ey} \tag{4}$$

The value $N_\alpha = C_{N\alpha}\bar{q}S_{ref}$ is the normal force coefficient per unit angle of attack, and near the gravity turn, the angle of attack is defined as

$$\alpha = \phi_y + \frac{\dot{z}_I}{V} - \frac{V_w}{V} \tag{5}$$

where V_w is the lateral wind velocity as shown in Figure 1. It is assumed that $\dot{\phi}_y = \omega_y$ and $\tan^{-1}\frac{x}{V} \approx \frac{x}{V}$ if $x \ll V$.

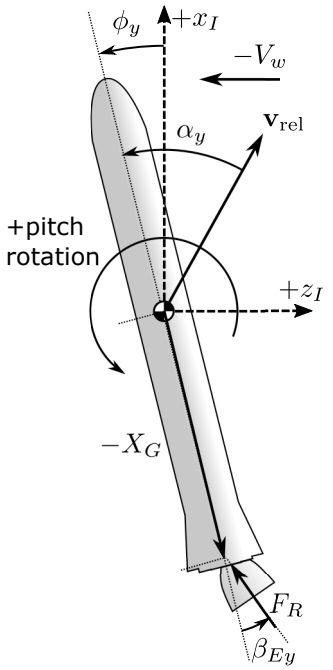

Figure 1. Linearized Vehicle Dynamics

Note that by definition the gravity turn, or reference trajectory, is a zero alpha trajectory, so $\phi_y = \dot{z}_I = V_w = 0$ implies that $\alpha = 0$. The body frame acceleration and quasi-inertial (or trajectory-relative) acceleration are related by

$$\ddot{z}_B = \ddot{z}_I + \bar{g}\phi_y \tag{6}$$

where $\bar{g}$ is the mean axial acceleration including the effects of drag. The quasi-inertial frame arises in the standard approach to linearizing the ascending dynamics of a rocket.[1]

It can be shown that for the longitudinal dynamics described by Equation 3 and with the control law in Equation 2 with $k_z = 0$, a suitable set of gains to achieve a specified control bandwidth and damping ratio ω_c, ζ_c are given by

$$k_p = \frac{I_{yy}\omega_c^2 + N_\alpha X_{cp}}{-X_G F_R} \tag{7}$$

$$k_d = \frac{I_{yy} 2\zeta_c \omega_c}{-X_G F_R}. \tag{8}$$

The resultant closed-loop system has 3 rigid-body poles: two, usually complex, are the rotation mode, and there is a single pole that represents the translation mode (normal to the reference trajectory). This translation pole is commonly called the *drift root*, since it represents the first-order dynamics of the vehicle velocity with respect to the reference trajectory. For pure PD feedback, this pole is neutrally stable.

In the absence of angle of attack or accelerometer feedback, the gains in Equations 7 and 8 provide an aerodynamic (low frequency) gain margin of approximately

$$\mathrm{GM}_a = 20 \log_{10} \frac{X_G F_R k_p}{N_\alpha X_{cp}}, \tag{9}$$

so it is typical to select ω_c to be sufficiently large that $\mathrm{GM}_a \geq 6\,\mathrm{dB}$. Most production launch vehicle autopilots use some variant of scheduled PD control, along with digital filters for elastic stabilization and loop shaping to increase phase margin and compensate for sloshing propellant and actuator dynamics. A small amount of integral gain can be employed to increase robustness to external disturbances such as thrust vector misalignment.

Using Equations 4 and 6 with pure accelerometer feedback, the control law takes the form

$$\beta_c = -\frac{m_T}{m_T - k_z F_R} \left(k_p \phi_y + k_d \omega_y + k_z \frac{N_\alpha}{m_T} \alpha \right) \tag{10}$$

since the sensed acceleration

$$\ddot{z}_s = -\frac{N_\alpha}{m_T} \alpha - \frac{F_R}{m_T} \beta_c - X_s \dot{\omega}_y. \tag{11}$$

For simplicity it can be assumed that $X_s = 0$; that is, the accelerometer is located at the instantaneous center of mass. In this case, the control law can be rescaled to an equivalent α-feedback law;

$$\beta_c = -k'_p \phi_y - k'_d \omega_y - k_\alpha \alpha. \tag{12}$$

2.1 Idealized Load Relief Laws

Hoelker[2] and others[3,4] derived fundamental control principles for a rigid body rocket from these observations, which allow selection of the gain k_z or k_α in order minimize (in the sense of the transfer function final value theorem) the quasi-steady variable of interest. The derivation of these results is lengthy and is omitted here, but the conditions are summarized as follows:

1. Load-minimum control. A limiting case where $k'_p = 0$ and the vehicle is stabilized using α feedback only. In this configuration, the vehicle will turn into a steady-state wind, and the drift root is *unstable*. This is not necessarily problematic for short durations of the ascent flight, so long as the attitude and path deviations are acceptable in nonlinear, time-domain simulation.

2. Drift-minimum control. This choice of gain minimizes the vehicle steady state acceleration relative to the trajectory, or $\ddot{z}_I(t \to \infty)$ in response to a wind input and corresponds to the case where the drift root is in the origin. It can be shown somewhat tediously that if the control law is written in the form of

   $$\beta_c = -(1 - \kappa) k'_p \phi_y - k_d \omega_y - \kappa k'_p \alpha, \tag{13}$$

   that is, by first designing the proportional and derivative gains according to Equations 7 and 8 and then apportioning some angle-of-attack feedback, that the drift-minimum control occurs at approximately $\kappa \approx 0.4$ for a typical launch vehicle near maximum dynamic pressure. In this case there exists a convenient closed-form expression for the steady-state angle of attack due to wind.[1]

3. Attitude-error minimum control. This gain selection minimizes the vehicle attitude error due to a steady-state wind, and is a useful design compromise. While transient loads due to wind are reduced, the vehicle will reach a drift velocity equal to the lateral wind velocity. It is therefore similar to PD control but results in lower aerodynamic bending moments. This control scheme has convenient analytical properties in that it fixes the location of the drift root. In the ideal case, the attitude response to a wind input is identically zero due to pole-zero cancellation.

These gain choices are idealized under the assumptions of a rigid vehicle and a steady-state wind, but it should be noted that time constants for "steady state" may be on the order of the entire launch trajectory! In addition, useful loads reductions are difficult to realize in practice, particularly due to stability concerns with the use of accelerometer feedback, so a compromise solution is determined via gain optimization and simulation analysis. Reliable direct angle of attack sensing at high velocities was demonstrated as early as the 1960s on the X-15 aircraft,[5] but despite the emergence of various pressure-based sensor suites (e.g., 5-hole and flush air data systems), none have been shown reliable and accurate enough in the critical transonic regime, and are subject to even aeroelastic errors as they must be located on the extreme forward end of the vehicle.

2.2 Saturn I/I-B and Space Shuttle

Both the Saturn I/IB and Space Shuttle ascent flight control systems used direct accelerometer feedback.[3,6–8] In the case of the Saturn IB, load relief was flight tested and shown to provide measurable reductions in transient loads, but it was equally important to compensate for lateral trajectory drift. Filtering of bending dynamics was a limiting factor for the Saturn launch vehicles, and despite being baselined for the Saturn V, load relief was eventually deleted prior to the launch of AS-501 in 1967. This decision was made in part due to analog filter hardware limitations, late changes in the definition of the winds environments, and concerns that the critical bending moments for Saturn V were dominated by the thrust vectoring loads.[9,10]

NASA's Space Shuttle employed a sophisticated design approach, but still relied on direct accelerometer feedback. The feedback scheme improved upon the Saturn design by incorporating a gyro rate input which was filtered to compensate for the angular acceleration term appearing in Equation 11. A reference acceleration function provided an error signal that drove the vehicle normal acceleration to its pre-launch design profile. This, combined with day-of-launch wind biasing, was used to allow some flexibility in the trajectory design while maintaining adequate loads margins, which were determined via coupled loads analysis and expressed in terms of a multivariate boundary coined a "squatcheloid". Due to the presence of wings on the Space Shuttle Orbiter, the vehicle trajectory was designed as a zero lift, not zero angle of attack, profile, and a supplemental force-balancing system was used in the elevon hydraulics to reduce elevon hinge moment loads during ascent.[6] The trajectory design amounts to a redefinition of the reference chord for zero angle of attack and does not change the interpretation of the flight control architecture.

The Shuttle design and analysis process suffered from the same difficulties as were encountered earlier in the Saturn program, in that body bending, particularly in the lateral (N_y or sideslip) channel, required aggressive filtering to stabilize and limited the achievable bandwidth. As the vehicle was upgraded and modified, for example in 1996 with the introduction of the Super Light Weight Tank (SLWT), a change in the vehicle structural characteristics elicited a significant risk assessment process by the flight control team.[11]

The efficacy of the Shuttle design approach was markedly clear on the first flight of STS-1 in 1981, where a confluence of modeling errors led to an anomalous ascent trajectory, increasing aerodynamic loading on the vertical tail to the point of nearly inducing structural failure. Despite many other errors in the as-flown versus pre-flight predicted flight control performance, the vehicle's load relief law closely tracked the reference angle of attack profile.[6]

2.3 Ares I/I-X and Space Launch System

The Ares I launch vehicle was developed during NASA's Constellation program, and an anti-drift law was demonstrated on the Ares I-X flight test vehicle in 2009.[12] This flight control law extended the concept of accelerometer feedback by using a simultaneous force and moment balance approach, and was designed to control trajectory errors early in the boost phase. The design used two first-order linear observers to estimate and counteract external forces and moments.

During the development of the Ares I launch vehicle, the Ares I-X anti-drift law was modified to include a load relief function and allow improved flexibility in gain scheduling.[13,14] Due to the low-frequency longitudinal bending modes and challenging aerodynamics of the Ares I, however, the performance of the Ares I load relief law was limited even after applying extensive numerical gain and filter optimization. It was noted during the development that due to the use of active damping (phase stabilization) for the first bending mode, employing load relief has the effect of decreasing the first bending mode damping for the closed-loop system. This has a potential unintended consequence of actually increasing bending loads. However, after much design effort it was shown that mean rigid-body $\bar{q}\alpha_T$ could be reduced about 7% through the use of a load relief algorithm. Comparative analyses on similar large launch vehicles has shown that a reduction of 5%-15% is typical.

NASA's Space Launch System (SLS) improved upon the Ares I design by decoupling the force and moment balance components of the algorithm into a pair of Disturbance Compensation Algorithms (DCA), described in detail elsewhere.[15] This design approach has the advantage of providing good load reduction in high dynamic pressure phases of flight, but can also provide compensation for external moment disturbances, particularly those due to a loss of engine thrust or from asymmetric burnout of the solid rocket motors. An early implementation of the SLS DCA improved the quality of the disturbance estimates through the use of nonlinear observers, but it was eventually shown, somewhat unsurprisingly, that the nonlinear observer offered no net benefit when its bandwidth was necessarily reduced for stability in the presence of structural dynamics.

3 IMPROVED METHODS

The continued emphasis on reducing structural mass and increasing launch availability has led to an interest in alternative load relief methods that do not require high-risk emerging sensor technologies. As mentioned previously, direct air data sensing has not been shown to be feasible and reliable for launch vehicles, and such sensor schemes are complex, can be contaminated by pre-launch weather events, and are difficult to reconcile with the high reliability requirements typical of a space booster. As such, it is useful to consider what improved capability can be obtained from existing software, range measurements, and inertial instruments.

Since the development of acceleration feedback load relief schemes in the 1950s, the capability of onboard avionics and inertial sensors has markedly improved. In fact, a fairly low-cost GPS-aided strapdown INS or comparable navigation-grade inertial system can provide angle-of-attack

estimates (excluding wind) with errors on the order of a few tenths of a degree.

3.1 Navigation Errors

A brief analysis can be used to illustrate the sensitivity of angle of attack estimates to navigation errors. Consider the angle of attack and sideslip given by

$$\begin{bmatrix} \alpha \\ \beta \end{bmatrix} = \begin{bmatrix} \tan^{-1} \frac{w}{u} \\ \sin^{-1} \frac{v}{V} \end{bmatrix} \tag{14}$$

where the body frame velocity components are related to the navigation frame components by the North-East-Down (NED)-to-body transformation

$$\begin{bmatrix} u \\ v \\ w \end{bmatrix} = \mathbf{T}^{BN}(t)\mathbf{v}^N \tag{15}$$

and $\mathbf{v}^N$ is the navigated velocity in the navigation frame. Expanding in terms of small perturbations δu, ... and assuming that $u_0, V_0 \gg \delta u$, etc.,

$$\begin{bmatrix} \alpha_0 + \delta\alpha \\ \beta_0 + \delta\beta \end{bmatrix} = \begin{bmatrix} \tan^{-1} \frac{w_0}{u_0} \\ \sin^{-1} \frac{v_0}{V_0} \end{bmatrix} + \begin{bmatrix} 0 & 0 & \frac{1}{u_0(t)} \\ 0 & \frac{1}{V_0(t)} & 0 \end{bmatrix} \begin{bmatrix} \delta u \\ \delta v \\ \delta w \end{bmatrix} \tag{16}$$

and

$$\begin{bmatrix} u_0 & & \delta u \\ v_0 & + & \delta v \\ w_0 & & \delta w \end{bmatrix} = \mathbf{T}_0^{BN} \left(\mathbf{I} - \mathbf{\Theta}^{\times} \right) \begin{bmatrix} v_{N0} & & \delta v_N \\ v_{E0} & + & \delta v_E \\ v_{D0} & & \delta v_D \end{bmatrix} \tag{17}$$

where the subscript 0 indicates the nominal trajectory and

$$\mathbf{\Theta} = \begin{bmatrix} \delta\phi \\ \delta\theta \\ \delta\psi \end{bmatrix} \tag{18}$$

are the navigation tilt errors. It is noted that the nominal turning rate $\dot{\mathbf{T}}_0^{BN}$ is nearly constant.

The aerodynamic angle errors are given by

$$\begin{bmatrix} \delta\alpha \\ \delta\beta \end{bmatrix} = \begin{bmatrix} 0 & 0 & \frac{1}{u_0(t)} \\ 0 & \frac{1}{V_0(t)} & 0 \end{bmatrix} \left(\mathbf{T}_0^{BN} \left(\mathbf{I} - \mathbf{\Theta}^{\times} \right) \begin{bmatrix} v_{N0} & & \delta v_N \\ v_{E0} & + & \delta v_E \\ v_{D0} & & \delta v_D \end{bmatrix} - \begin{bmatrix} u_0 \\ v_0 \\ w_0 \end{bmatrix} \right). \tag{19}$$

Note that the quantity

$$\mathbf{T}_0^{BN} \begin{bmatrix} v_{N0} \\ v_{E0} \\ v_{D0} \end{bmatrix} - \begin{bmatrix} u_0 \\ v_0 \\ w_0 \end{bmatrix} = \mathbf{0} \tag{20}$$

so expanding and discarding second-order terms,

$$\begin{bmatrix} \delta\alpha \\ \delta\beta \end{bmatrix} = \begin{bmatrix} 0 & 0 & \frac{1}{u_0(t)} \\ 0 & \frac{1}{V_0(t)} & 0 \end{bmatrix} \mathbf{T}_0^{BN}(t) \left(\begin{bmatrix} \delta v_N \\ \delta v_E \\ \delta v_D \end{bmatrix} + \mathbf{v}_{N0}^{\times} \begin{bmatrix} \delta\phi \\ \delta\theta \\ \delta\psi \end{bmatrix} \right) \tag{21}$$

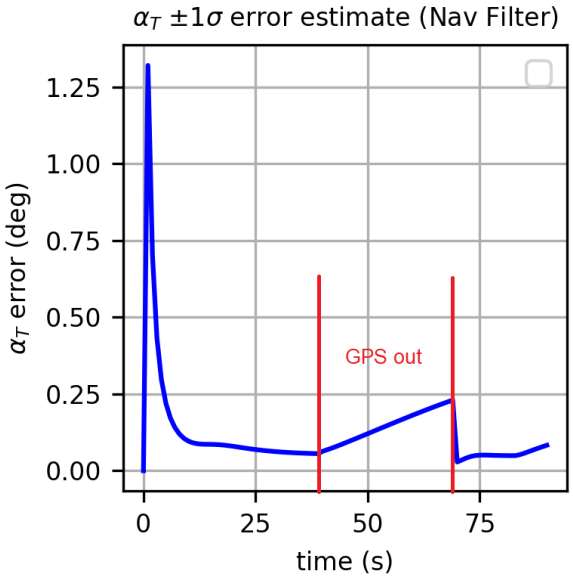

Figure 2. Inertial α Covariance Estimate with GPS Outage

Assembling these in a covariance transformation

$$\mathbf{Z}_{\alpha\beta} = \begin{bmatrix} 0 & 0 & \frac{1}{u_0(t)} \\ 0 & \frac{1}{V_0(t)} & 0 \end{bmatrix} \mathbf{T}_0^{BN}(t) \left[\begin{array}{c|c} \mathbf{I} & \mathbf{v}_{N0}^{\times} \end{array} \right] \tag{22}$$

the aerodynamic angle covariance is

$$\mathbf{P}_{\alpha\beta} = \mathbf{Z}_{\alpha\beta} \mathbf{P}_{\mathbf{v}\Theta} \mathbf{Z}_{\alpha\beta}^T \tag{23}$$

for the covariance matrix $\mathbf{P}_{\mathbf{v}\Theta}$ associated with the navigation error state vector

$$\boldsymbol{\delta} = \left[\begin{array}{cccccc} \delta v_N & \delta v_E & \delta v_D & \delta\phi & \delta\theta & \delta\psi \end{array} \right]^T . \tag{24}$$

A navigation covariance analysis of a typical instrument package on a representative boost trajectory is shown in Figure 2 using a standard 21-state Extended Kalman Filter (EKF) to estimate instrument and alignment errors. The navigation system in this example is a tactical-grade IMU using ring laser gyros (RLGs) combined with civilian-grade GPS aiding and a prelaunch alignment phase, although similar results can be obtained with better instruments and no GPS aiding. The 1σ error covariance in the total angle of attack estimate is generally within 0.25 degree throughout the portion of the trajectory most critical for loads, around 40-70 seconds after liftoff. A GPS outage is induced during this period to illustrate the capability of an inertial-only solution during this critical flight regime. In fact, the dominant errors, not represented here, are due to mounting deformations and vehicle bending, as well as sensor-to-body misalignments.

As can be seen, inertial measurements alone can provide very good estimates of the components of the angle of attack relative to a quiescent atmosphere. The dominant error terms are inversely proportional to the vehicle velocity. Combined with pre-launch winds data stored online and updated just prior to launch, a composite synthetic angle of attack estimate can be constructed in the flight software that is of sufficient accuracy to reduce loads without relying on external measurements.

3.2 Day-of-Launch (DOL) Wind Biasing

There exists significant precedent for the use of range winds measurements for prelaunch wind biasing, particularly in the NASA space launch community. This approach was used extensively for trajectory shaping during the Space Shuttle program by combining mean monthly winds (a predictive product) with day-of-launch updates to the vehicle software tables, whereas in the Saturn program mean monthly winds were used to shape the first-stage open-loop attitude command profile.[3]

The principal challenges in the use of Day-of-Launch wind biasing, and the associated process of Day-of-Launch I-Load Update (DOLILU) is quantifying the spatial and temporal uncertainties that arise in the prelaunch measurement data set, particularly for simulation-based risk assessment. Shuttle experience suggests that the adequacy of the real-time data set can be determined by executing the DOLILU analysis process twice, for example, once two hours prior to flight and again one hour prior to flight. It is noted that there is a significant software and procedure development cost, risk, and software verification impact incurred by adopting DOLILU in that it fundamentally modifies a critical flight software parameter just before launch. That is, from a loads and dynamics perspective, incorrect DOLILU is significantly worse than no DOLILU at all.

There have been numerous approaches adopted to model uncertainty in winds aloft and turbulence for simulation, the former now standardized through the use of range-specific Global Reference Atmosphere Model (GRAM), developed by NASA's Marshall Space Flight Center. Unfortunately however, at major test ranges, there exists little statistical data on the accuracy of measured winds versus actual winds, since there is seldom a "truth reference" to quantify the errors in measurements derived from balloon soundings. However, there have been efforts to quantify sounding errors via comparative analysis of Doppler Radar Wind Profiler (DRWP) measurements at lower altitudes, which generally indicates good correlation over a few hours' timeline. For the production simulations discussed in this paper, a conservative model is derived from Monte Carlo GRAM profiles corrupted by a linear combination of Gauss-Markov errors and random walk (Figure 3), with parameters chosen based on experience at a particular range.

3.3 Load Relief Guidance

Assuming that an estimate of the vehicle angle of attack is available online, a guidance scheme can be constructed that modulates the vehicle steering commands to reduce angle of attack much in the way that direct inner-loop feedback provides a load relief function. In the architecture proposed in this paper, the load relief law is constructed as an outer-loop command generation scheme, and therefore is called a "guidance" law as compared with a flight control law, since the flight control law structure is unmodified from its basic proportional-derivative form.

While there exist numerous automated methods to develop optimal gains for linear controllers such as those used on missiles and rockets, a classical multi-loop structure allows for a convenient functional decomposition of the guidance (steering) and flight control components. When integrated, as in the case of the SLS autopilot, the dimensionality and complexity of the numerical gain and filter optimization problem is markedly increased. Relegating the load relief function to a steering command can offer a simplified approach to gain tuning as well as stability analysis, as will be shown. In addition, inner-loop gain adaptive control[16] can be employed without modulating the gain of the load relief component(s).

Revisiting the pitch plane dynamics described in Equations 3 and 4, Equation 5 can be differen-

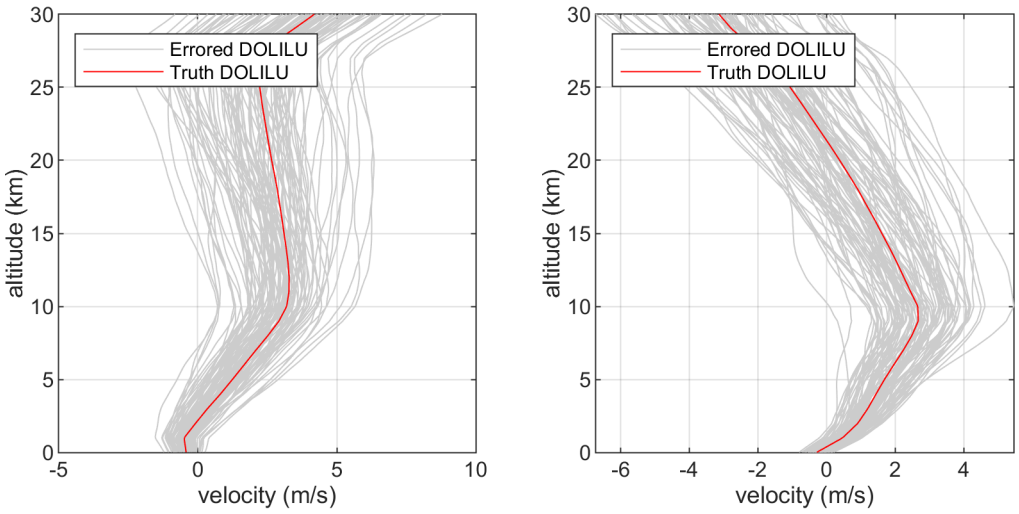

Figure 3. Example of DOLILU Winds Error Model

tiated assuming that the forward and wind velocities are approximately constant;

$$\dot{\alpha} = \omega_y + \frac{\ddot{z}_I}{V}. \tag{25}$$

The angle of attack rate can be rewritten in terms of the body frame acceleration (Equation 6) as

$$\dot{\alpha} = \omega_y + \frac{\ddot{z}_B}{V} - \frac{\bar{g}\phi_y}{V}. \tag{26}$$

Using a method similar to the traditional two-loop missile autopilot,[17] let the α-dynamics be described by the open loop system

$$\dot{\alpha} = u_\alpha \tag{27}$$

where u_α is the control variable given by

$$u_\alpha = k_{p\alpha}\alpha + \int_0^t k_{i\alpha}\alpha(\tau)\mathrm{d}\tau \tag{28}$$

such that the α-dynamics open-loop transfer function is

$$G'_\alpha(s) = \frac{k_{p\alpha}}{s} + \frac{k_{i\alpha}}{s^2} \tag{29}$$

and the closed-loop transfer function is

$$G_\alpha(s) = \frac{k_{p\alpha}s + k_{i\alpha}}{s^2 + k_{p\alpha}s + k_{i\alpha}}. \tag{30}$$

Assuming that angle-of-attack rate can be controlled directly as in Equation 27, the coefficients $k_{i\alpha}$, $k_{p\alpha}$ can be chosen to meet some performance specification, for example, $k_{i\alpha} = \omega_\alpha^2$ and $k_{p\alpha} = 2\zeta_\alpha\omega_\alpha$ where ω_α, ζ_α are the natural frequency and damping of the α-control mode. In this proportional-integral form, there will be some overshoot in the α response due to the zero in

Equation 30 if this feedback law is used with a time-varying reference signal $\alpha_c(t)$, e.g., an angle-of-attack command. This can be alleviated by introducing a command filter

$$\frac{\alpha_c'(s)}{\alpha_c(s)} = \frac{k_{i\alpha}}{k_{p\alpha}s + k_{i\alpha}} \tag{31}$$

which will invert the zero in the alpha transfer function. For load relief, however, the reference command is zero and this complication is avoided.

It then remains to implement a steering law that results in angle of attack rate control. By equating the expressions in Equation 26 and 27, it is clear that if the autopilot is commanded to follow a body angular rate of

$$\omega_{yc} = \frac{\bar{g}\phi_y - \ddot{z}_B}{V} + k_{p\alpha}\alpha + \int_0^t k_{i\alpha}\alpha(\tau)\mathrm{d}\tau \tag{32}$$

the angle of attack error will be driven to zero asymptotically. This steering law forms the basis of the proposed load relief guidance scheme.

It is apparent from Equation 6 that the first term in Equation 32 compensates the angle of attack rate due to *acceleration* normal to the trajectory, and this term can be constructed in a variety of ways. The most straightforward is to use the gravity turn error ϕ_y and an estimate of the acceleration at the center of mass. For low-velocity portions of the trajectory, the contribution of this term can be large, leading to bending stability issues concerns when using sensed acceleration $\ddot{z}_s$. Conversely, the decrease in gain with increasing velocity is favorable for bending stability. The former concern can be alleviated by only employing the steering law when V is sufficiently large. Alternatively, if the vehicle aerodynamic parameters and mass properties are known reasonably well *a priori*, a measurement of $\ddot{z}_B$ can be replaced with

$$\hat{\ddot{z}}_B = -\frac{N_\alpha\alpha + F_R\beta_c}{m_T}. \tag{33}$$

For most launch vehicles, the bare airframe is statically unstable, requiring the proportional control signal for longitudinal stability as suggested in Equation 9. In contrast to a tail-controlled missile with neutral static stability, the rate command in Equation 32 must be combined with a kinematically consistent attitude command. The autopilot error signals are constructed as

$$\theta_e = \chi - \theta_y + \int_0^t \omega_{yc}(\tau)\mathrm{d}\tau \tag{34}$$

$$\dot{\theta}_e = \dot{\chi} - \omega_y + \omega_{yc} \tag{35}$$

where $\phi_y = \chi - \theta_y$, the gravity turn error with respect to some reference (such as launch site vertical). The last terms can be blended in and out to allow a transition from and back to the gravity turn. It is noted that this control law is by definition a load-minimum control law for any values of $k_{p\alpha}$, $k_{i\alpha} > 0$. The authors conjecture that for $k_{p\alpha} = k_{i\alpha} = 0$, the nulling of angle-of-attack rate provides a equivalent outer-loop mechanization of drift-minimum control, where $\dot{\alpha} \to 0$ as $t \to \infty$.

Since this feedback law forms a two-loop structure used to construct autopilot commands, it is necessary from a control design standpoint that they be sufficiently separated in bandwidth for stability. Implementation and analysis suggests that the classical rule of thumb of about a factor of three separation of ω_α and the control frequency ω_c is sufficient for outer-loop stability margins.

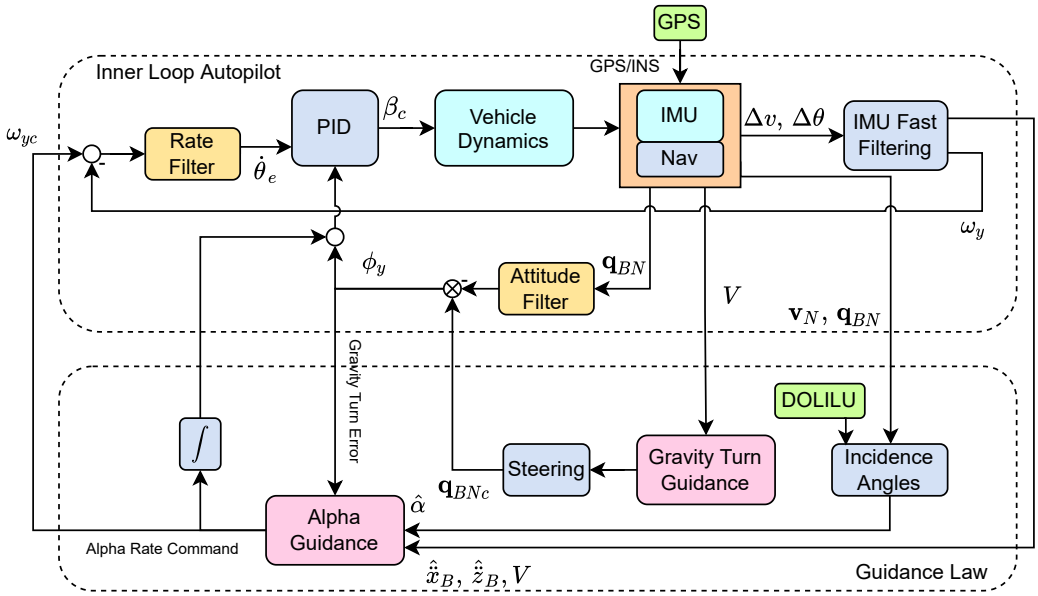

Figure 4. Integrated GN&C Architecture With Load Relief

A block diagram of the integrated GN&C system including the gravity turn guidance and load relief steering law is shown in Figure 4. In the software mechanization, the navigation system provides body-to-navigation frame quaternion which is decomposed into small error angle Euler sequence for filtering and processing. For stability analysis, the autopilot open-loop transfer function can be analyzed at the classical β_c loop break, or at the load relief rate command ω_{yc}. Conveniently, the load relief law is still a linear feedback law, and classical frequency-domain linear stability analysis techniques are applicable. A frequency-domain analysis will be summarized in Section 4.

3.4 Acceleration Estimation

The load relief law steering law presented in the preceding Section and the classical load relief laws detailed in Section 2 assumed that an estimate of the acceleration at the center of mass was available. In the Saturn era, the parasitic effect of the angular acceleration due to the location of the instrument package was incorporated into the design trade space, and the Shuttle flight control law compensated for this effect via a differentiation filter. In the present implementation, the differentiation filter concept is extended using an IMU fast filtering algorithm, so called due to its implementation at a rate typically greater than 100 Hz in flight software. By operating in discrete time directly on the IMU ΔV, $\Delta\theta$ measurements typical of a strapdown IMU, a filtered estimate of the body angular rates and CG acceleration can be constructed directly if an estimate of the center of mass is known *a priori*.

The IMU fast filtering algorithm derives the center of mass acceleration in the body frame $\dot{\mathbf{v}}_B$ using the relationship

$$\dot{\mathbf{v}}_B = \dot{\mathbf{v}}_s - \dot{\omega}_s^{\times}\hat{\mathbf{r}}_s - \omega_s^{\times}\omega_s^{\times}\hat{\mathbf{r}}_s \tag{36}$$

where $\dot{\mathbf{v}}_s$ is the sensed acceleration at the IMU and $\hat{\mathbf{r}}_s$ is an estimate of the sensor location with

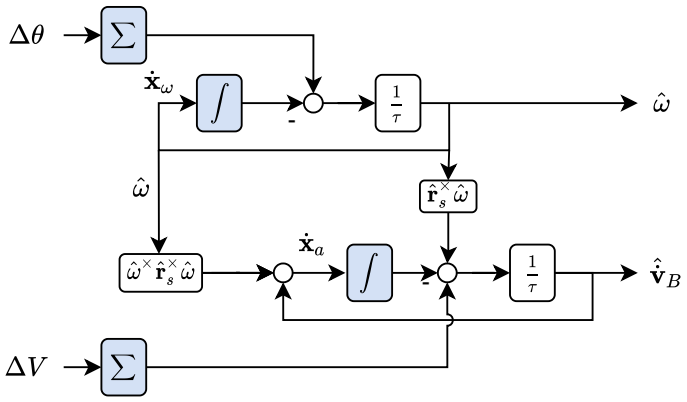

Figure 5. IMU Fast Filtering Block Diagram

respect to the center of mass, determined from table lookup. It is assumed in this expression that the motion of the center of mass due to burning propellant is negligible; that is, $\dot{\mathbf{r}}_s = \mathbf{0}$.

A schematic of the continuous form of the fast filtering algorithm is shown in Figure 5. This system consists of two first-order linear Luenberger observers connected by nonlinear operations that compensate for the dynamic terms arising in Equation 36, and is similar in structure to that employed in the SLS DCA algorithm.[15]

The state dynamics of the angular rate estimator are given by

$$\dot{\mathbf{x}}_\omega = -\frac{1}{\tau}\mathbf{x}_\omega + \frac{1}{\tau}\sum \Delta\theta \tag{37}$$

$$\hat{\omega} = \dot{\mathbf{x}}_\omega \tag{38}$$

and the acceleration estimator dynamics are

$$\dot{\mathbf{x}}_a = \frac{1}{\tau}\left(\sum \Delta V + \hat{\mathbf{r}}_s^\times\hat{\omega} - \mathbf{x}_a\right) + \hat{\omega}^\times\hat{\mathbf{r}}_s^\times\hat{\omega} \tag{39}$$

$$\hat{\mathbf{v}}_B = \dot{\mathbf{x}}_a - \hat{\omega}^\times\hat{\mathbf{r}}_s^\times\hat{\omega}. \tag{40}$$

Each scalar element of the estimator in Equation 37 has the continuous time transfer function

$$H(s) = \frac{s}{\tau s + 1}, \tag{41}$$

a first-order high-pass filter. Letting $s = K\frac{z-1}{z+1}$ (the Tustin bilinear transform) we find that

$$H[z] = \frac{K\,(z-1)}{(\tau K + 1)\,z - \tau K + 1} = \frac{b_1 z - b_1}{z + a_0} \tag{42}$$

with

$$a_0 = \frac{1-\tau K}{\tau K + 1},\; b_1 = \frac{K}{\tau K + 1},\; K = \frac{2}{T_s} \tag{43}$$

where T_s is the sampling period. The discrete transfer function in Equation 42 has the difference equation

$$y_k = -a_0 y_{k-1} + b_1 u_k - b_1 u_{k-1} = -a_0 y_{k-1} + b_1 \Delta u_k. \tag{44}$$

In this form, the digital estimator state equations can implemented at a fixed sample rate (corresponding to the IMU output sample rate) as

$$\hat{\mathbf{v}}_{Bk}^{-} = -a_0 \hat{\mathbf{v}}_{Bk-1} - b_1 \hat{\mathbf{r}}_s^{\times} \hat{\omega}_{k-1} \tag{45}$$

$$\hat{\omega}_k = -a_0 \hat{\omega}_{k-1} + b_1 \Delta\theta \tag{46}$$

$$\hat{\mathbf{v}}_{Bk}^{+} = \hat{\mathbf{v}}_{Bk}^{-} + b_1 \left(\Delta V + \hat{\mathbf{r}}_s^{\times} \hat{\omega}_k \right) + (1 + a_0)\, \hat{\omega}_k^{\times} \hat{\mathbf{r}}_s^{\times} \hat{\omega}_k. \tag{47}$$

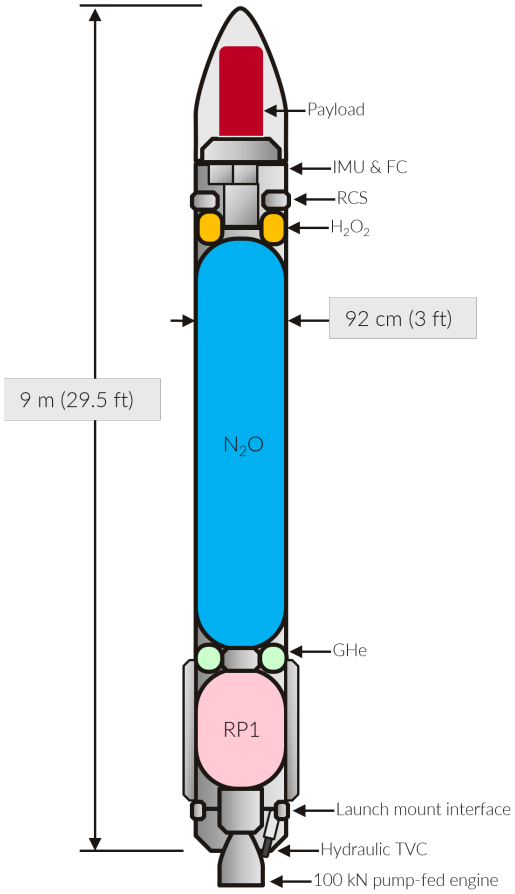

Figure 6. SSTV Layout

noting the intermediate update of the angular rate estimate $\hat{\omega}_k$. In implementation, a time constant τ is chosen such that the -3 dB frequency of the differentiator filter is well below the sample rate Nyquist frequency and does not amplify noise outside of the usable flight control system bandwidth, while maintaining a phase response close to the ideal $+\frac{\pi}{2}$. An example with IMU measurements at 100 Hz uses $\frac{1}{\tau} = 2\pi \cdot (20\,\text{Hz})$. It is worth mentioning that equivalent coefficients b_1, a_0 can be generated using a matched z-transform method with slightly improved phase response compared with the Tustin transformation.

4 ANALYSIS AND SIMULATION

The proposed load relief guidance scheme has been implemented and tested in a production launch vehicle flight dynamics simulation, Dynamic Environment for Launch Trajectory Analysis (DELTA) using the Agile Vehicle Stack (AVS) MATLAB-based flight software environment. DELTA is a modular simulation architecture that incorporates the effects of vehicle rigid-body dynamics, servo-inertial coupling, propellant slosh, and airframe bending in an high-fidelity dynamics engine based on a Lagrangian formulation of the equations of motion.[1]

The vehicle for which load relief was evaluated is known as Single Stage Test Vehicle (SSTV) (Figure 6), a concept vehicle derived from research studies and now used in GN&C system trades to avoid program and proprietary information sensitivity. The SSTV vehicle is a single-stage liquid-propellant booster with a thrust-vectored 100 kN engine, having approximately 13000 kg mass at liftoff and 7000 kg of propellant. The vehicle is nominally flown southeast from the Pacific Spaceport Complex (PSCA) on Kodiak Island,

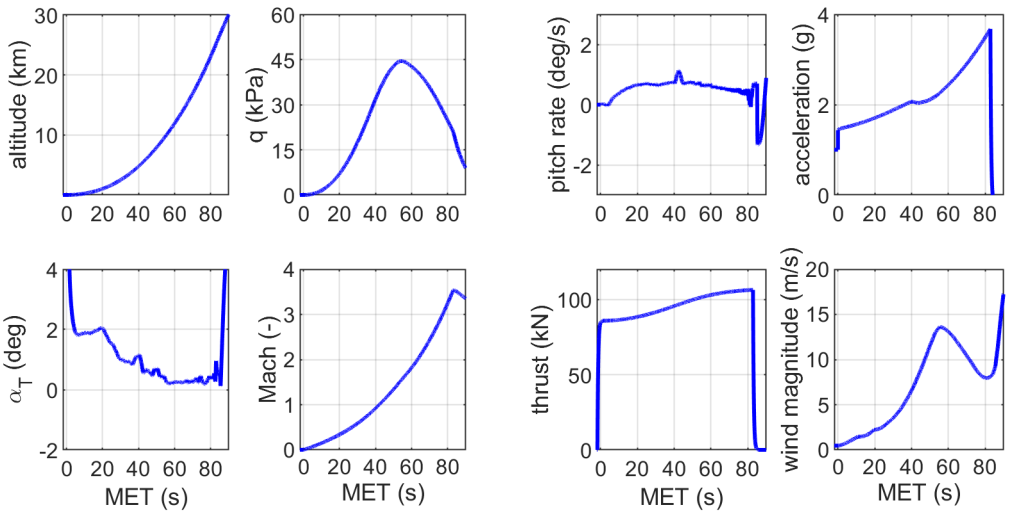

Figure 7. SSTV Launch Trajectory Overview

Alaska, and reaches an altitude of about 26 km at burnout with a velocity of 1.1 km/s (Mach 3.5). The total duration of the powered flight is 85 seconds with a peak dynamic pressure occurring at 55 seconds after liftoff (Figure 7). For illustration, the nominal vehicle trajectory is designed for a quiescent atmosphere, and the vehicle ascends into an initial southwesterly wind after an azimuth alignment maneuver and pitch-over occurring at 4 seconds after liftoff.

The gain-scheduled proportional-derivative flight control law (with integral feedback) is implemented in software at 50 Hz with guidance and steering (including the load relief law) discretized and updated at 10 Hz. Roll control is provided by a two-stage monopropellant reaction control system and a phase plane control law. The boost phase attitude profile is provided by a lookup table, which is used to approximate the ideal gravity turn tilt angle time history $\chi(t)$ through offline trajectory optimization using a sequence of cubic splines.

For illustration purposes, the load relief law is enabled at 40 seconds after liftoff and gains are increased to maximum over a five second window, and eventually are decreased again to zero after 30 seconds (MET=+70s). This time window is chosen to evaluate the algorithm performance in the critical region of maximum dynamic pressure and is not necessarily the optimal design for the present trajectory, which has not been designed with wind biasing. In the discussion that follows, the analysis results are summarized only in this flight regime.

4.1 Linear Stability Analysis

A linear stability analysis of the inner-loop autopilot and outer-loop load relief steering law is shown in Figure 8. In this high-fidelity linear model, the vehicle's planar rigid-body dynamics are incorporated with a spring-mass model of the sloshing propellant tanks, vehicle flexibility, servo-inertial coupling, and the hydraulic actuator subsystem.[18] The inner-loop control frequency is $\omega_c = 2\pi \cdot (0.35\,\mathrm{Hz})$ and the load relief control frequency is $\omega_\alpha = 2\pi \cdot (0.12\,\mathrm{Hz})$ with a target damping ratio of $\zeta_\alpha = 0.707$. For the inner loop autopilot, it is observed that increasing the inner-loop phase margin directly correlates with outer-loop phase margin, as is expected in the classical sense; therefore, the inner-loop target damping is increased to about $\zeta_c = 1.4$. While this value is used to

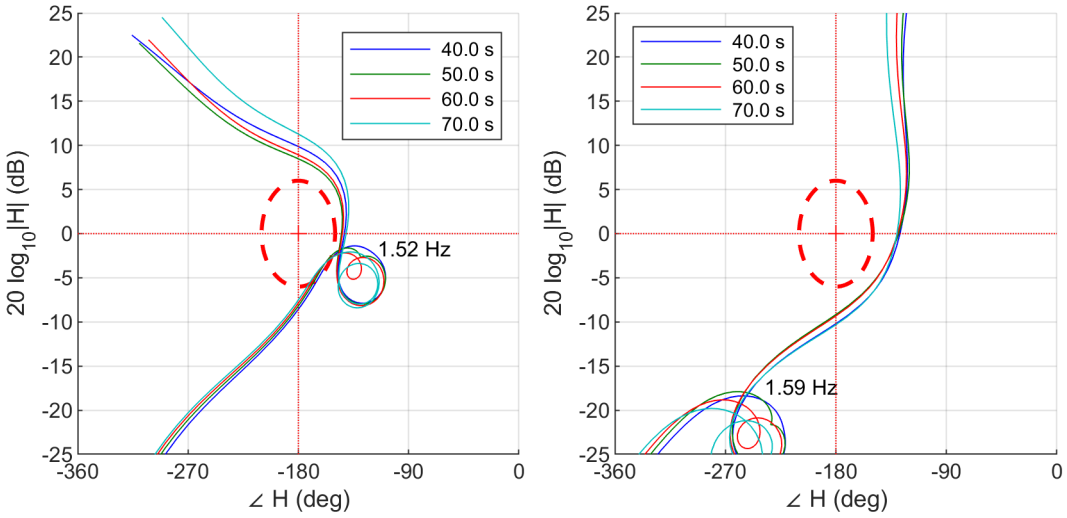

Figure 8. Linear Stability Analysis (pitch inner loop, left; pitch load relief, right)

parameterize the rigid-body gain, the effective damping is closer to to $\zeta = 0.8$, owing to the phase margin degradation of body bending filters.

In the depicted analysis, body bending effects are omitted, although the filter dynamics are included in the autopilot loop. The longitudinal bending modes of the subject vehicle are generally greater than 7 Hz, and while appearing most significantly in the accelerometer channel, are of no consequence to the dynamic response with appropriate filtering. All body bending is gain stabilized and the autopilot rate filters have a $-3\,\mathrm{dB}$ frequency of about 5 Hz. The effects of slosh are evident in the open loop; although the sloshing propellant modes are phase stable and well-damped at about 4% of critical, they appear in both the autopilot loop via the rate channel and in the aerodynamic control loop due to coupling through the accelerometer. Gain and filter design is parameterized to target approximately 30 degrees of phase margin and 6 dB of gain margin in the inner loop, and these are depicted as an ellipsoid in the magnitude-phase plane. The aerodynamic control loop is adjusted to have a phase margin and gain margin of about 45 degrees and 10 dB, respectively.

A transient response analysis based on the linear model is shown in Figure 9. Simulation testing has shown that these transient response curves correlate well with the nonlinear, time-varying vehicle dynamics for both the autopilot inner loop and the load relief feedback scheme. An initial attitude error of $\phi_y = 1\,\mathrm{deg}$ is shown (left), indicating that gain scheduling is successful in ensuring a response that is relatively invariant to changing vehicle mass properties and aerodynamics. The vehicle angle of attack in response to a step $25\,\frac{\mathrm{m}}{\mathrm{s}}$ gust (right) further confirms that the angle-of-attack control performance is consistent and scales with the vehicle forward velocity for a constant lateral wind velocity.

4.2 Monte Carlo Analysis

The efficacy of a load relief law can seldom be evaluated based on the performance of single design cases, but can be quantified statistically through Monte Carlo analysis. The present design was evaluated in the DELTA simulation environment using a representative set of vehicle dispersions, including variations of vehicle dry mass, loaded propellant, propulsion performance, and propellant

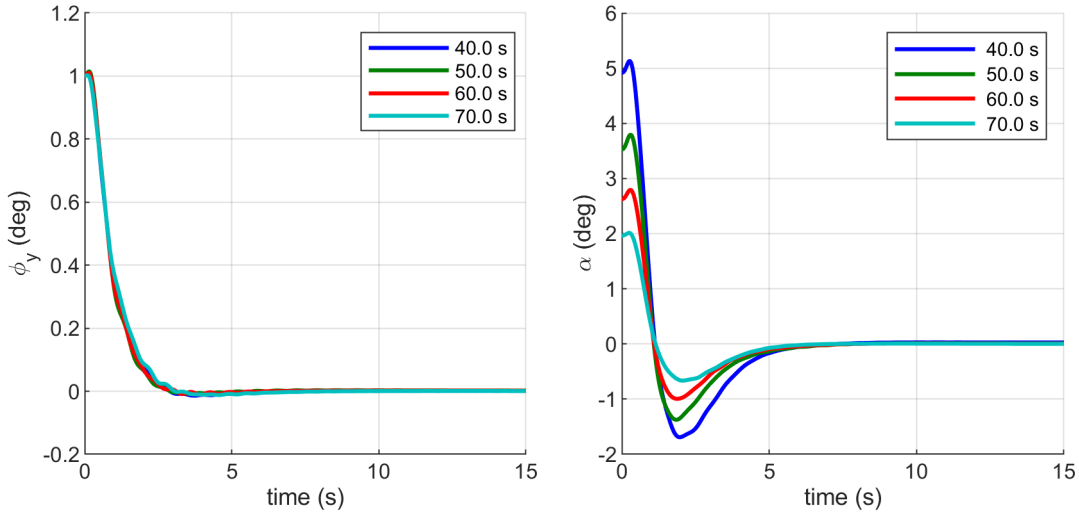

Figure 9. Linear Transient Analysis (attitude tracking, left; 25 m/s gust response, right)

sloshing parameters. The environments model is derived from GRAM 2016's PSCA range reference atmosphere (RRA) combined with a standard ground winds boundary layer model, and the aforementioned error model is employed for DOLILU tables. A medium-fidelity GPS/INS sensor model is used, representative of a specific commercially available IMU, and incorporates the effects of sensor misalignment, accelerometer and gyro bias, bias instability, and random walk. The GPS model is consistent with an unlimited-altitude civilian receiver (SPS) and includes both stochastic and geometric errors.

For statistical analysis, the simulation includes three sets of 2,000 run Monte Carlo samples: (1) a nominal trajectory with load relief disabled and no wind biasing; (2) a nominal trajectory with load relief enabled and all error models included; and (3) a nominal trajectory with load relief enabled but no DOLILU errors (e.g., perfect knowledge of winds aloft). The latter case is used to assess the sensitivity of wind measurement errors on the load relief performance. 2,000 Monte Carlo runs are required to produce valid statistics[19] at the 90% confidence level (10% consumer risk or Type II error probability) using a Gaussian 3σ order statistic for the variables of interest, primarily the rigid-body load indicator $\bar{q}\alpha_T$. Identical random number seeds are used to ensure accurate case-to-case comparisons.

A comparison of rigid-body load indicators for the load relief off case (left) and load relief on case (right) is shown in Figure 10. Clearly, engagement of a load-minimum equivalent steering solution at MET=+40s has the effect of rapidly decreasing the angle of attack as the dynamic pressure increases on the trajectory, substantially reducing the load. It is noted that while the relatively late engagement of the algorithm illustrates the performance, a production design might blend in load relief earlier in the trajectory. Due to the use of DOLILU, the small angle of attack error slightly increases the load indicator in the nominal case (Figure 10, right). This is expected and is offset by the load reduction of the ensemble.

A statistical comparison of the load relief performance is shown in Table 1. The efficacy of the present algorithm is indicated by the significant reduction in the mean and 99.865% quantile values of the rigid-body load indicator. Although engagement of the algorithm occurs just prior to

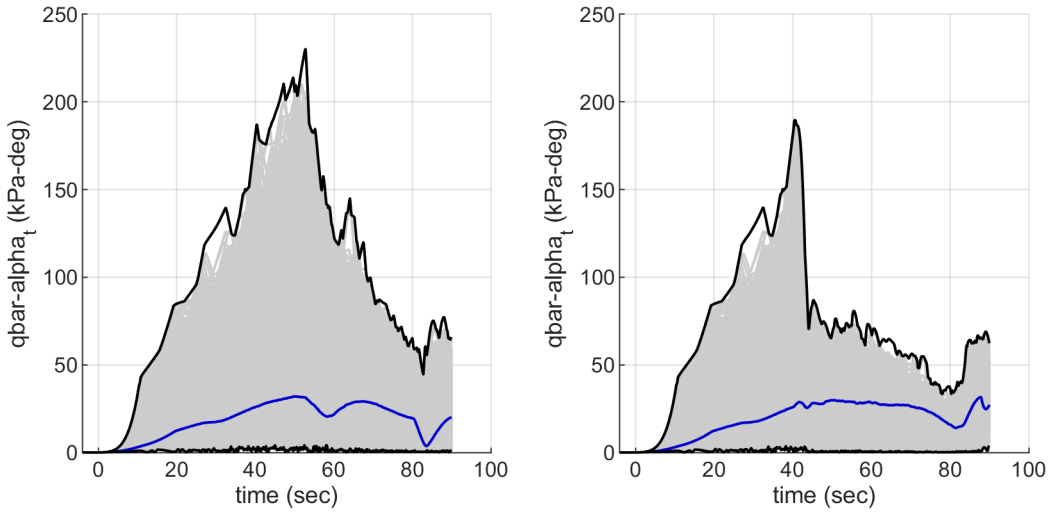

Figure 10. Rigid Body Load Indicator (no LR, left; LR with all errors, right)

Output Metric (10% CR)	LR off	LR on	Change from Baseline
Mean rigid body load indicator, $\bar{q}\alpha_T$	108.7 kPa-deg	78.9 kPa-deg	-38%
$\bar{q}\alpha_T$ 99.865% high	216.5 kPa-deg	188.5 kPa-deg	-15%
α at Mach=1, 99.865% high	3.3 deg	1.3 deg	-54%
Pitch rate, ω_y 99.865% high	2.2 deg/s	3.0 deg/s	+36%

Table 1. Monte Carlo Statistics, 2000 run samples

transonic, the rapid decrease in angle of attack is reflected as a significant reduction at Mach 1. Such reductions are beneficial to mitigate induced environments on secondary structures and hardware, particularly the effects of aeroacoustics and buffet on sensitive avionics and payload components.

The effects of DOLILU errors on the angle of attack estimation performance is shown in Figure 11. In the absence of DOLILU table errors; e.g., perfect knowledge of the winds aloft, the inertially estimated angle of attack is affected only by GPS and IMU errors, and is in family with the prior navigation covariance analysis. The introduction of temporal and spatial errors in the prelaunch winds table introduces an additional 1-2 degrees of angle of attack error, including the aforementioned effect on the nominal case. The large errors early in the trajectory are due to the change in wind direction as the vehicle ascends after liftoff at relatively low velocity. The ground winds are not captured in the DOLILU process.

5 CONCLUSIONS

In this paper, a novel load relief guidance and steering approach has been presented that reformulates the classical inner-loop acceleration feedback scheme into an outer-loop command scheme under the assumption that angle of attack estimates can be derived from a combination of prelaunch winds measurements and inertial velocity measurements. This approach is derived under the same

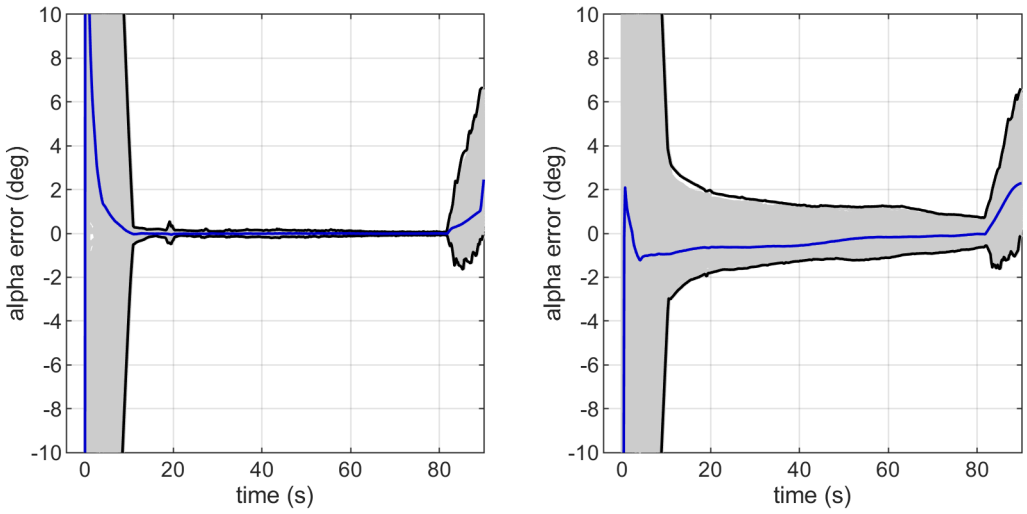

Figure 11. Angle of Attack Estimation Performance (perfect DOLILU, left; errored DOLILU, right)

linearization assumptions used for dynamic analysis of boost vehicles, and as such can be analyzed for frequency-domain stability margins and transient performance using industry-standard linear models. The multi-loop design approach is similar to that used for missile systems and may make the overall GN&C design more tractable by separating the design, analysis, and optimization steps via a sequential loop closure methodology.

Linear navigation covariance analysis and Monte Carlo simulation suggests that acceptable angle-of-attack estimation performance can be obtained even with relatively inexpensive GPS-aided IMUs at the high end of the "tactical" product spectrum, and for a typical boost vehicle trajectory, the angle of attack errors are dominated by the variations in the wind field from the time of measurement to the time of launch. This implies that investment in (1) improved statistical models of errors in range balloon soundings and (2) improving the fusion of DRWP and balloon measurements into the DOLILU process could considerably improve launch availability when paired with algorithms that take advantage of this data.

The reader is cautioned that although the simulated results are very favorable, the allowable accelerometer feedback gain is higher than could be obtained with an orbital launch system since the vehicle bending frequencies are higher owing to the stiff structure of the SSTV rocket. In addition, the nature of the simulated mission is not sensitive to staging conditions or injection errors. While the load relief algorithm did not have a significant effect on the trajectory shape, a reduction of the load relief bandwidth may be required for multistage systems so as to reduce the drift effects of what is, in essence, a load-minimum feedback scheme.

ACKNOWLEDGMENTS

The authors are grateful to John Wall of NASA MSFC (Dynamic Concepts, Inc.) for many years of insightful discussion regarding load relief, and to Lee Yang (Draper) for his thorough analysis of load relief options during NASA's Constellation program. In addition, the support of the NASA Engineering and Safety Center (NESC) GN&C Technical Discipline Team (TDT) is gratefully acknowledged, particularly Neil Dennehy (NASA GSFC), Aron Wolf (JPL), and Tannen VanZwieten

(NASA KSC). This work was performed under contract to NESC (NASA LaRC 80LARC17C0003) via subcontract with Analytical Mechanical Associates, Inc.

REFERENCES

[1] Barrows, T. and Orr, J., Dynamics and Simulation of Flexible Rockets, Elsevier (Academic Press), 2021.

[2] Hoelker, R.F., "Theory of Artificial Stabilization of Missiles and Space Vehicles With Exposition of Four Control Principles," NASA TN D-555, NASA Marshall Space Flight Center, June 1961.

[3] Haeussermann, W., "Description and Performance of The Saturn Launch Vehicle's Navigation, Guidance, and Control System," NASA TN D-5869, NASA Marshall Space Flight Center, July 1970.

[4] Jaggers, R., "Derivation of a Drift Minimum/Loads Minimum Control Law for Booster, Atmospheric Flight," NASA Johnson Space Center 5-2950-1-HOU-278, May, 1971.

[5] Wolowicz, C.H. and Gossett, T.D., "Operational and Performance Characteristics of the X-15 Spherical, Hypersonic Flow-Direction Sensor," NASA TN D-3070, November 1965.

[6] Olsen, L.M and Sunkel, J.W., "Postflight Evaluation of the Shuttle Guidance, Navigation, and Control During Powered-Ascent Flight Phase," J. Guidance, Vol. 6, No. 6, pp. 418-423.

[7] Schleich, W.T., "Shuttle Vehicle Configuration Impact on Ascent Guidance and Control," J. Guidance, Vol. 7, No. 3., pp. 338-346.

[8] Ryan, R., "Fundamental Concepts of Structural Loading and Load Relief Techniques for the Space Shuttle," NASA TM X-64684, NASA Marshall Space Flight Center, August 1972.

[9] Frosch, J. and Vallely, D., "Saturn AS-501/S-IC Flight Control System Design," J. Spacecraft, Vol. 4, No. 8, 1967, p. 1003-1009.

[10] Orr, J., Wall, J., and Dennehy, N., "The Enduring Legacy of Saturn V Launch Vehicle Control Design Principles & Practices," 70th International Astronautical Congress, IAC-19-9-D6.2, 21-25 October 2019.

[11] Altenbach, R., NASA STS SSD96D0526, *STS Bending Flight Mechanics Data Book*, September 1996.

[12] "Control Algorithm and Parameters for the Ares I-X Flight Test Vehicle," AI1-SYS-CAP-V4.00, NASA Exploration Systems Mission Directorate, October 21, 2009.

[13] Jang, J. et al., "Ares I Flight Control System Design," AIAA Guidance, Navigation, and Control Conference, Toronto, Ontario, Canada, AIAA 2010-8442, August 2010.

[14] Wall, J., "Analytical Presentation of the Ares I Anti-Drift / Load-Relief Flight Control Option," NASA Marshall Space Flight Center / EV41, Nov 9, 2009.

[15] Orr, J., Wall, J., VanZwieten, T., and Hall, C., "Space Launch System Ascent Flight Control Design," American Astronautical Society Guidance, Navigation, and Control Conference, Breckenridge, CO, February 2014, AAS 14-038.

[16] Wall, J., Orr, J., and VanZwieten, T., "Space Launch System Implementation of Adaptive Augmenting Control," American Astronautical Society Guidance, Navigation, and Control Conference, Breckenridge, CO, February 2014, AAS 14-051.

[17] Menon, P.K. and Yousefpor, M., "Design of Nonlinear Autopilots for High Angle of Attack Missiles," AIAA Guidance, Navigation, and Control Conference, AIAA 96-3913, July 1996. 3.3

[18] Orr, J. et al., "State Space Implementation of Linear Perturbation Dynamics Equations for Flexible Launch Vehicles," AIAA Guidance, Navigation and Control Conference, Chicago, Illinois, AIAA-2009-5962, August 2009.

[19] Hanson, J., and Beard, B., Applying Monte Carlo Simulation to Launch Vehicle Design and Requirements Analysis, NASA Technical Report TP-2010-216447, NASA Marshall Space Flight Center, Sep. 2010.